FREE Webinar:

ClearLLab LS: A New CE-IVD Orientation Tube to Guide You Through Diagnosis of Hematolymphoid Malignancies

Dr. Katherina Psarra from the Immunology Dept. at Evangelismos Hospital, Athens and Dr. Michael Kapinsky, one of Beckman Coulter's clinical flow cytometry experts, will present:

- Determination of immunologically defined leukocyte subpopulations
- Immunophenotyping of hematological malignancies
- Influence of instrument and dye performance characteristics on your phenotyping results
- Panel design driven by: dye brightness vs antigen density; spillover-spreading and co-expression patterns

Thursday | July 12, 2018
3pm CEST | 9 am EDT

Receive a FREE eCasebook when you Register Here

BECKMAN COULTER Life Sciences

CURRENT PROTOCOLS A Wiley Brand

WILEY

Received: 15 September 2017 | Accepted: 6 April 2018
DOI: 10.1002/jcb.27040

RESEARCH ARTICLE

WILEY Journal of Cellular Biochemistry

The intranuclear PEX domain of MMP involves proliferation, migration, and metastasis of aggressive adenocarcinoma cells

Yuka Okusha[1] | Takanori Eguchi[1,2] | Chiharu Sogawa[1] | Tatsuo Okui[3] | Keisuke Nakano[2,4] | Kuniaki Okamoto[1] | Ken-Ichi Kozaki[1]

[1] Department of Dental Pharmacology, Graduate School of Medicine, Dentistry and Pharmaceutical Sciences, Okayama University, Okayama, Japan

[2] Advanced Research Center for Oral and Craniofacial Sciences, Graduate School of Medicine, Dentistry andPharmaceutical Sciences, Okayama University, Okayama, Japan

[3] Department of Oral and Maxillofacial Surgery, Graduate School of Medicine, Dentistry and Pharmaceutical Sciences, Okayama University, Okayama, Japan

[4] Department of Pathology and Medicine, Graduate School of Medicine, Dentistry and Pharmaceutical Sciences, Okayama University, Okayama, Japan

Correspondence
Takanori Eguchi, DDS, PhD, Department of Dental Pharmacology, Okayama University, 2-5-1, Shikata-cho, Kita-ku, Okayama city, 700–8525, Japan
Email: eguchi@okayama-u.ac.jp

Funding information
Ryobi Teien Memorial Foundation;
A Ryobi Teien Memorial Foundation Grant;
Japan Society for the Promotion of Science, Grant numbers: JP17K11642, JP17K17895, JP26293067, JP26670815;
Okayama Univ. Gender Equality Grant, Molecular Imaging Micro Dose Phase 0 Grant, Start-up Grant for Young Scientists

Abstract

Members of matrix metalloproteinase (MMP) family promote cancer cell migration, invasion, and metastasis through alteration of the tumor milieu, intracellular signaling pathways, and transcription. We examined gene expression signatures of colon adenocarcinoma cell lines with different metastatic potentials and found that rapidly metastatic cells powerfully expressed genes encoding MMP3 and MMP9. The non-proteolytic PEX isoform and proteolytic isoforms of MMPs were significantly expressed in the metastatic cells in vitro. Knockdown of MMP3 attenuated cancer cell migration and invasion in vitro and lung metastasis in vivo. Profound nuclear localization of MMP3/PEX was found in tumor-stroma marginal area. In contrast, MMP9 was localized in central area of subcutaneous tumors. Overexpression of the PEX isoform of MMP3 promoted proliferation and migration of the rapidly metastatic cells in vitro. Taken together, the non-proteolytic PEX isoform of MMPs locating in cell nuclei involves proliferation, migration, and subsequent metastasis of aggressive adenocarcinoma cells.

KEYWORDS
cancer metastasis, nuclear MMP, non-proteolytic MMP, PEX domain, tumor stroma

1 | INTRODUCTION

Metastasis is a critical phenomenon in cancer. Over time, malignant cancer cells undergo clonal evolution, which promotes their diversity and heterogeneity, as well as therapy resistance.[1–3] In addition, it has been proposed that highly evolved clones of cancer cells are resistant to selective

Abbreviations: CTGF, connective tissue growth factor; HSP, heat shock protein; IHC, Immunohistochemistry; MMP, matrix metalloproteinase; PEX, hemopexin-like repeat; RNAi, RNA interference; siRNA, small interfering RNA.

pressure by the immune, chemo- and radiation therapies. Although previously considered to be mutually exclusive models, it is recently considered that genetic evolution and cancer stem cell models can be harmonized in three related biological fields; tumor genetics, epigenetics and pathways, and microenvironment.[3] Matrix metalloproteinases (MMPs) represent the most prominent family of proteinases associated with tumorigenesis and regulators of the tumor microenvironment.[4,5] MMPs have also been reported to be potent biomarkers of tumor progression as well as one of the causal factors that promote multiple processes of tumorigenesis, including oxidative stress-dependent DNA damage and chromosomal instability, epithelial-to-mesenchymal transition (EMT),[6] migration and invasion of cancer cells,[7] angiogenesis, and metastasis.[4,5,8] Canonical proteolytic roles for MMPs is to cleave substrate proteins at extracellular space. Proteolysis of extracellular matrix (ECM) and intercellular adhesion molecules by MMPs enable cells to migrate and invade and to release cytokines, chemokines, and growth factors that activate their receptors and intracellular signaling pathways. In addition to those indirect activations of the extracellular factors, MMPs also directly alter activities of growth factors, cytokines, and chemokines by proteolysis. For example, MMPs are able to cleave connective tissue growth factor (CTGF/CCN2) and then release VEGF leading to angiogenesis.[9] Another study showed that MMPs and a disintegrin and metalloproteinases cleave membrane-bound heparin-binding EGF-like growth factor (HB-EGF) and release soluble HB-EGF, which binds to cells and stimulates EGFR/ERBB signaling.[10]

Intracellular and nuclear roles for MMPs have been recently discovered. We showed that MMP3 possesses nuclear localization signals and can translocate into cellular nuclei, in which MMP3 can bind to chromatin proteins and DNA leading to transcriptional regulation of *CTGF/CCN2* gene.[11] MMP3 is composed of a protease domain, a hinge region, and a C-terminal hemopexin-like repeat (PEX) domain, which is non-proteolytic (see later figure). We recently showed that a PEX isoform of MMP3 activate some members of heat shock protein (HSP) genes,[12] which can contribute to anti-apoptosis and drug resistance. MMP3 can interact with heterochromatin proteins, members of the chromobox protein family that involve transcriptional and chromosomal control.[11–13] MMPs also involve oxidative stress, DNA damage, and chromosome instability in cell nuclei. Intranuclear MMP2 and MMP9 activities have been shown to cleave PARP-1 and XRCC1, nuclear matrix proteins, thus promoting oxidative DNA damage and apoptosis in an ischemic injury model.[14] MMP3-induced EMT and genomic instability have been shown to be mediated by small GTPase Rac1b and a reactive oxygen species in breast adenocarcinoma and pancreatic cancer,[6,15] indicating potent roles for MMPs in proteotoxic and genotoxic stress.

MMPs appear to be appropriate target molecules in treatments of aggressive types of cancers. Although more than 50 MMP inhibitors have been investigated in clinical trials for various cancers, all of those trials failed.[8] However, the involvement of intracellular and non-proteolytic roles for MMPs in cancer have not well-investigated yet.

In the present study, we first investigated gene expression of MMPs correlated with metastatic phenotype of colon cancer cells. We then assessed nuclear localization of the PEX domain of MMP3 and MMP9 in primary and lung-metastatic tumors and their roles in proliferation, migration, invasion, and metastasis of the aggressive cancer cells.

2 | MATERIALS AND METHODS

2.1 | Cells

Colon26 (also known as colon26), LuM1, and NM11 cells were maintained in RPMI1640 with 10% FBS supplemented with penicillin, streptomycin, and amphotericin B.[16–18]

2.2 | Comprehensive gene expression analysis and bioinformatics

Cells were cultured for 3 days and total RNA was extracted from cultured cells using the AGPC method with Trizol (Molecular Research Center, Cincinnati, OH). Concentration and quality (A260/A280) of total RNA were determined. cDNA was synthesized from 0.1 μg of total RNA using a Low Input Quick Amp Labeling Kit (Agilent Technologies, Santa Clara, CA), then hybridized to probes of a SurePrint G3 Mouse GE 8×60 K v.2 Microarray system (Agilent Technologies). Gene expression and ratios were analyzed using MeV 4.0 software (http://www.Tm4.org/mev.html). Functional annotation clustering and pathway analysis were performed with LuM1 genes expressed at a 10-fold or higher level as compared to the NM11 and Colon26 cells ($P < 0.05$) using DAVID Bioinformatics Resources 6.8. Relative expression levels in LuM1 or NM11 to the levels in Colon26 were shown in heat maps and bar graphs.

2.3 | RNAi

Cells were transfected with small interfering RNA (siRNA) targeting mRNA of *Mmp3* or *Mmp9* (ON-TARGETplus SMARTpool siRNA; Thermo Fisher Scientific, Rockford, IL), or non-targeting double strand RNA (dsRNA) (siGENOME Control Pool Non-Targeting siRNA) at a final concentration of 50 nM using DharmaFECT 1 (Thermo Fisher Scientific, Rockford, IL). Cells were cultured for 48 h before RT-qPCR, Western blot, migration assay, invasion assay, and subcutaneous injection and for 72 h before

zymography. For analysis of culture supernatant, cells were cultured for 48 h in serum-containing medium and subsequently 24 h in serum-free medium. To examine mRNA levels in tumors, total RNA was extracted from subcutaneous tumors on the day 10 after subcutaneous injection. Lung metastasis assay and immunohistochemistry (IHC) were performed on the day 20 after subcutaneous injection as depicted in Figure S2A.

2.4 | Real-time RT-qPCR

Total RNA preparation and RT-qPCR was carried out as described previously.[11,12] The miRNeasy mini kit (Qiagen, Hilden, Germany) was used with DNase (Qiagen). Total RNA concentration was measured by using a microspectrometer K2800 (Beijing Kaiao, Beijing, China). cDNA synthesis was carried out by using iScript™ cDNA Synthesis Kit (Bio-Rad, Richmond, CA). Specific primer pairs for *Mmp3, Mmp9, Actb,* and *Gapdh* were used as follows: mMmp3Fw, 5′-ACC AAC CTA TTC CTG GTT GCT GCT and mMmp3Rv, 5′-ATG GAA ACG GGA CAA GTC TGT GGA[19]; mMmp9Fw, 5′-CAG CCG ACT TTT GTG GTC TT and mMmp9Rv, 5′-GCT TCT CTC CCA TCA TCT GG[20]; mGapdhFw, 5′-ACC ACA GTC CAT GCC ATC AC and mGapdhRv, 5′-TCC ACC ACC CTG TTG CTG TA[21]; mActb-Fw, 5′-AAC GAG CGG TTC CGA TG and mActb-Rv, 5′-GGA TTC CAT ACC CAA GAA GGA.[20] Realtime PCR was carried out using iQ SYBR Green PCR mixture (Bio-Rad). Relative mRNA levels to *Actb* or *Gapdh* mRNA levels were quantified by the ΔΔCt method using the formula as follows: fold change $= 2^{-\Delta\Delta Ct}$. PCR was carried out in triplicate and mean values were calculated with the mean ± S.D. of biological triplicates.

2.5 | Migration and invasion assays

Migration and invasion assays were performed as previously described.[17] Uncoated and Matrigel-coated culture systems (Becton Dickinson, Franklin Lakes, NJ) were used for in vitro migration and invasion assays, respectively. For knockdown experiments, cells were transfected with siRNA and then cultured for 48 h before re-seeding to upper chambers. Cells were seeded at concentrations of 5×10^4 per an upper chamber of a Transwell® 24-well (Corning, Corning, NY) for the migration assay and of 2.5×10^4 per an upper chamber of a Transwell® 24-well for the invasion assay. Cells transfected with PEX-overexpressing or control plasmids were seeded at concentrations of 5×10^4 per an upper chamber of a Transwell® 24-well for the migration assay and of 1.6×10^4 per an upper chamber of a Transwell® 24-well for invasion assay. Cells that migrated or invaded through the pores to the lower surface of filter were fixed, stained using Diff-Quick stain (Sysmex, Kobe, Japan) and counted after 6 h of migration period or 19 h of invasion period for knockdown experiments, and after 0, 12, and 24 h for comparison of different cell lines. To evaluate the effects of the transfection, percentages of migrated and invaded cells relative to the control were calculated.

2.6 | Cell proliferation

Cells were transfected with siRNA or plasmid DNA and then seeded at a concentration of 3.8×10^3 cells/well in a 96-well plate on the day 2 after transfection. Number of cells at 1-4 days post-transfection period were counted by using Countess automated cell counter (Invitrogen, Carlsbad, CA). Floid® cell imaging station (ThermoFisher Scientific) was used for photomicrography.

2.7 | Allogeneic transplantation

All animal experiments were performed according to the guidelines for care and use of laboratory animals approved by Okayama University and the Japanese Pharmacological Society. Subcutaneous allogeneic transplantation was performed as previously described,[17] with 5.0×10^5 cells transplanted subcutaneously into a side abdominal wall of each 6 to 7-week-old BALB/c mouse. Twenty days after transplantation, subcutaneous tumors and lungs were resected, then fixed with Bouin's fluid. Nodules larger than 0.5-mm-diameter were counted.

2.8 | Casein and gelatin zymography

For zymography of non-transfected cells, cells were inoculated at a concentration of 2×10^6 cells into 60-mm culture dishes in 4 mL of RPMI1640 containing 10% FBS and cultured overnight, then incubated in serum-free medium for 24 h. Cell culture supernatants were concentrated 20 times using an Amicon filtration tube (for MW 10 000). Cells were washed with PBS, collected using a cell scraper, and lysed in RIPA buffer containing a protease inhibitor cocktail (Sigma-Aldrich, St Louis, MO), then further lysed by homogenization (25-gauge needle, 10 strokes) and incubated for 30 min on ice. Lysates were centrifuged at 12 000*g* for 20 min to remove debris and supernatants were used as cell lysates. Twenty microgram of cell lysates or 4 μg of cell culture supernatants were mixed with an SDS sample buffer and $CaCl_2$ (5 mM final concentration), then applied to 10% acrylamide gel containing copolymerized 0.1% gelatin (Cosmo Bio, Tokyo, Japan). For zymography with knockdown experiments, cells were cultured in six-well plates. At 48 h after transfection, medium was replaced with serum-free medium and cells were cultured for 24 h, then the supernatants were ultrafiltrated and concentrated as described above. Following a protein assay, 9 μg of the >10-kDa cell culture supernatant

was mixed with a 2× sample buffer (10 μL) and 1 μL of 50 mM $CaCl_2$, then separated on 10% acrylamide gels containing copolymerized 0.1% gelatin or 0.5% casein (CosmoBio, Tokyo, Japan). The gels were washed with wash buffer for 30 min at RT and incubated for 40 h in enzyme reaction buffer at 37°C. Coomassie Brilliant Blue staining was performed and photographs of the gels were obtained, then quantitative densitometric analysis was performed using Image J.

2.9 | Western blot analysis

Cells were seeded into six-well plates and transfected with siRNA using the procedure described above, then lysed in RIPA buffer as described above. Next, 30-μg protein samples were separated by SDS-PAGE on 10% poly-acrylamide gels and transferred to PVDF membranes. The membranes were blocked in Tris-buffered saline containing 0.05% Tween 20, 2.5% skim milk, and 2.5% BSA for 30 min at room temperature (RT). Each membrane was incubated with the primary antibody (1/1000) overnight at 4°C and subsequently incubated with horseradish peroxidase (HRP)-conjugate secondary antibodies against anti-rabbit IgG (GE Healthcare, Buckinghamshire, UK) (1/2000) for 1 h at RT in the blocking solution. Blots were visualized with a Clarity Western ECL Substrate (Bio-Rad).

2.10 | Antibodies

Rabbit monoclonal anti-PEX domain MMP3 antibody (EP1186Y, ab52915) and a rabbit polyclonal anti-MMP9 antibody (ab38898, full-length protein corresponding to mouse MMP9 was immunized) were purchased from Abcam.

2.11 | Immunohistochemistry

Excised tumor tissues were immediately fixed in Bouin's fluid, then dehydrated by passage through an ethanol series and embedded in paraffin. Samples were cut into 4-μm serial sections, which were then placed onto saline-coated slides. Deparaffinized sections were treated with methanol containing 0.3% H_2O_2 for 30 min to block endogenous peroxidase activity. Sections were then autoclave heated in 10 mM of citrate buffer solution (pH 6.0) for 10 min at 120°C for antigen retrieval. Blocking was performed using a Dako Chem Mate Envision Kit/HRP. Sections were incubated with the anti-MMP3 antibody (ab52915; 1/100) overnight at 4°C and subsequently with a secondary antibody against anti-rabbit IgG HRP-conjugated (K400211-2, EnVision+ Single Reagents, Dako) for 1 h at 4°C. IHC reaction products were visualized by use of a diaminobenzidine chromogen substrate. Samples were then counterstained with hematoxylin and observed with a BZ-X700 (Keyence, Osaka, Japan). For a negative control, sections were incubated with omission of the primary antibody under the same protocol.

2.12 | Immunofluorescence and confocal microscopy

For immunofluorescence staining, excised tumor tissues were immediately fixed in Bouin's fluid, then dehydrated by passage through an ethanol series and embedded in paraffin. Samples were cut into 4-μm serial sections, which were then placed onto saline-coated slides. Blocking was performed using a Dako Chem Mate Envision Kit. Sections were incubated with the anti-MMP3 antibody (ab52915; 1/100) and the anti-MMP9 antibody (ab38838; 1/500) overnight at 4°C and subsequently with a secondary antibody against anti-rabbit IgG (ab150076; 1/5000) for 1 h at 4°C. For a negative control, sections were incubated with omission of the primary antibody under the same protocol. After three washes with TBS, the mounting and DNA staining were performed by using ProLong gold AntiFade reagents with 4_,6-diamino-2-phenylindole (DAPI) (Molecular Probes, Invitrogen). Fluorescence images were taken using a confocal laser scanning microscopy LSM780 (Carl Zeiss, Oberkochen, Germany) at Central Research Laboratory, Okayama University Medical School. We defined four areas of a subcutaneous tumor as follows: the stromal as an outside of the tumor margin, the marginal as an area 0 to 30 μm apart from the tumor margin, the interior as an area 30 to 80 μm apart from the outside of the marginal area. According to this definition, MMP3/9 and/or DAPI positive cells in each area were counted using Image J. The nuclear MMP positive rate was calculated as follows: MMP3/9 and DAPI double positive nuclei per DAPI positive nuclei.

2.13 | Plasmid constructs and transfection

pFlag3-PEX-myc and pFlag3-myc were described previously.[22] These plasmid constructs were transfected using NEPA21 electroporator (NEPA Gene, Ichikawa, Japan). To optimize transfection condition and efficiency for LuM1, 10 different conditions of electroporation was tested. An optimized electroporation condition with 150V and 5 ms pulse twice was then used for plasmid transfection.

2.14 | Statistical analysis

Statistical significance was calculated using Microsoft Excel. Three or more mean values were compared using one way analysis of variance (ANOVA), while comparisons of two were done with an unpaired Student's *t*-test. $P < 0.05$ was considered to indicate statistical significance.

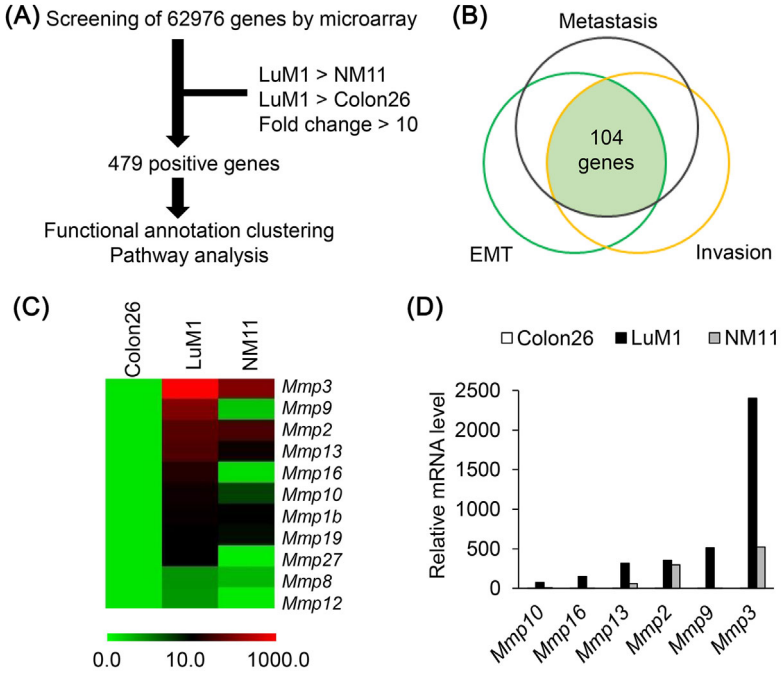

FIGURE 1 Transcriptome analysis revealed *Mmp* genes expressed in colon cancer cells with different metastatic potential. A, Flow chart of gene screening. Microarray screened 62976 genes. The 479 genes were expressed at more than 10-fold higher level in LuM1 as compared to NM11 and Colon26 cells. B, Venn diagram extracted 104 genes involved in invasion, EMT, and metastasis. C, Heat map analysis of *Mmp* gene family. The gene expression levels relative to the levels in Colon26 were shown. D, Expression levels of *Mmp* genes in LuM1, NM11, and Colon26 cells. The gene expression level of *Mmp3* in LuM1 was the highest among all *Mmp* gene family members, as well as compared to that in NM11 and Colon26 cells

3 | RESULTS

3.1 | Gene expression signatures and gene screening of high- and low-metastatic cancer cell lines

We first examined gene expression signatures of colon adenocarcinoma cell lines with different metastatic potentials in high-metastatic LuM1, low-metastatic NM11, and the parental Colon26 cells. To characterize these cell types with different invasive and metastatic potentials at gene expression levels, microarray analysis was carried out. (Raw data were submitted to the Gene Expression Omnibus (GEO) database repository; accession ID: GSE97166; Colon26, GSM2553008; LuM1, GSM2553009; NM11, GSM2553010.) Among the 62 976 genes tested, 479 genes were strongly expressed at a greater than 10-fold higher level in the metastatic LuM1 as compared to the low-metastatic lines (Figures 1A and S1). Functional annotation clustering and pathway analysis then revealed that the gene expression signature of LuM1 involved particular biological events in the extracellular microenvironment, cell adhesion, immunology, and protein interactions (Tables 1 and 2,). In addition, functional classification of those LuM1-specific genes indicated that these 104 genes specifically expressed in LuM1 involved cancer cell invasion, EMT, and metastasis (Figure 1B). These results indicated that more than a hundred metastasis-related genes involved metastatic, invasive, and transforming potential of the LuM1 cells. Among the 104 metastasis-related genes expressed specifically in LuM1 cells, several members of *Mmp* gene family, were profoundly expressed. We therefore examined *Mmp* expression signatures in the LuM1, NM11, and Colon26 cells. Of note, the gene expression level of *Mmp3* in the metastatic LuM1 was the highest among all *Mmp* gene family members and higher than that in Colon26 and NM11 (2400.9-fold and 4.6-fold, respectively, Figures 1C and 1D; S1C) . *Mmp9* was also expressed in the LuM1 at a high level, as compared to the low-metastatic Colon26 and NM11 (512.1-fold and 237.8-fold, respectively, Figure 1D).

These results indicate that *Mmp3* and *Mmp9* were profoundly co-expressed in the metastatic adenocarcinoma cells.

3.2 | Targeted knockdown of MMP3 attenuates proliferation, migration, and invasion of the metastatic adenocarcinoma cells

We next examined migration and invasion activities of metastatic LuM1 cells and low-metastatic NM11 cells, as well as of their parental low-metastatic adenocarcinoma cell

TABLE 1 Functional annotation clustering

Annotation cluster 1 enrichment score: 2.49	*P*-value
GO:0044421 extracellular region part	0.0010483
GO:0005576 extracellular region	0.0050501
GO:0005615 extracellular space	0.0064459
Annotation cluster 2 enrichment score: 2.11	*P*-value
GO:0007155 cell adhesion	0.0046972
GO:0022610 biological adhesion	0.0047962
GO:0016337 cell-cell adhesion	0.0213548
Annotation cluster 3 enrichment score: 1.90	*P*-value
GO:0006954 inflammatory response	0.00592
GO:0006952 defense response	0.0092881
GO:0009611 response to wounding	0.0107201
GO:0002252 immune effector process	0.0416591
Annotation cluster 4 enrichment score: 1.83	*P*-value
GO:0030246 carbohydrate binding	4.37E-04
GO:0030247 polysaccharide binding	0.0119368
GO:0001871 pattern binding	0.0119368
GO:0005539 glycosaminoglycan binding	0.0228992
GO:0008201 heparin binding	0.0477234

Genes expressed at a 10-fold greater level in LuM1 as compared to those in NM11 and Colon26 cells were analyzed.

line Colon26. LuM1 showed the highest levels of migration and invasion as compared to the other low metastatic lines (Figure 2A-C). We then examined siRNA-mediated knockdown of MMP3 and MMP9. Both MMP3 and MMP9 at mRNA levels were specifically and efficiently reduced by their targeted siRNA (Figures 2D and 2E). (Later figures show knockdown at protein levels). Yet the MMP3 siRNA increased the MMP9 mRNA level (Figure 2E) and, in contrast, the MMP9 siRNA increased the MMP3 mRNA level (Figure 2D), suggesting compensatory expression system of these essential MMPs. (Some mutual compensation was also seen in Western blotting and zymography as shown in later figures).

We next examined roles of MMP3 and MMP9 in regard to proliferation of LuM1 cells. The MMP3 siRNA (50 nM) tended to attenuate proliferation of the LuM1 cells whereas the MMP9 siRNA (50 nM) and MMP9/MMP3 siRNA mixture (each 25 nM) did not (Figure 2F and S2B). The MMP3 siRNA and MMP3/MMP9 siRNA attenuated the migration of LuM1 cells to 46.9% and 51.3%, respectively, of the level of the control (Figure 2G), and attenuated invasion to 71.0% and 59.7%, respectively (Figure 2H). The MMP9 siRNA attenuated migration of the LuM1 to 69.6%, which was a lesser effect as compared to MMP3-targeting, and did not alter invasion (Figures 2G and 2H).

These results indicate that MMP3 is a key protein in the proliferation, migration, and invasion of the aggressive adenocarcinoma cells.

3.3 | Targeted reduction of MMP3 and MMP9 attenuates primary and lung-metastatic tumorigenesis of the aggressive adenocarcinoma cells

We next examined whether knockdown of MMP3 and MMP9 could alter primary tumor development and lung metastasis of the LuM1 cells in the allogeneic transplantation experiments. As pilot studies, we tested sustainability of siRNA-mediated knockdown as follows. The RNAi effect on MMP9 was sustained for 96 h after transfection to LuM1 cells, as shown by gelatin zymography (Figure S2C). Of note, RNAi effects on *Mmp3* and *Mmp9* at mRNA levels were sustained in tumors in vivo even at day 10 after subcutaneous injection (Figure S2D). Using this knockdown system, we examined whether MMP3- and MMP9-targeting siRNA alter tumor development and metastasis. The weights of primary tumors were reduced by the MMP3 siRNA and the MMP9 siRNA on day 20 after the transplantation, as compared to the control (Figures 3A and 3B).

The number of metastatic nodules in lungs were significantly reduced by the MMP3 siRNA, the MMP9 siRNA and the MMP3/MMP9 siRNA, as compared to the control (Figures 3C and 3D). The weights of lungs bearing the metastatic nodules were significantly reduced by the MMP3 siRNA, the MMP9 siRNA, and the MMP3/MMP9 siRNA, as compared to the control (Figure 3E).

These results suggest that targeted knockdown of MMP3 and MMP9 reduce primary tumor development and subsequent metastasis of aggressive adenocarcinoma cells.

TABLE 2 Ranking of altered pathways in LuM1 as compared to NM11 and Colon26 cells

Category	Term	*P*-value
KEGG_PATHWAY	mmu04060:Cytokine-cytokine receptor interaction	0.0202
KEGG_PATHWAY	mmu04062:Chemokine signaling pathway	0.0253
KEGG_PATHWAY	mmu04142:Lysosome	0.0283
KEGG_PATHWAY	mmu04020:Calcium signaling pathway	0.0325

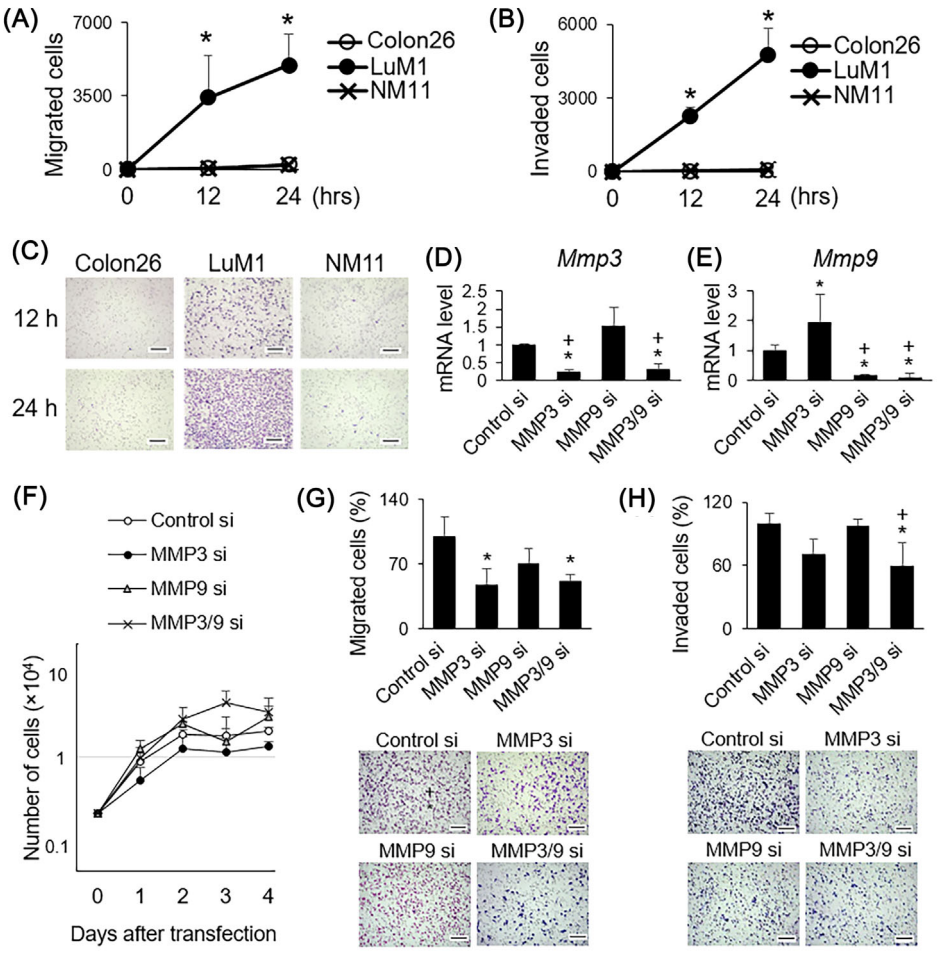

FIGURE 2 The roles of MMP3 and MMP9 in proliferation, migration, and invasion of the metastatic adenocarcinoma cells. A, Differential in vitro migration activities. Migrated cells per well was shown. The migration activity of LuM1 was higher than that of NM11 and Colon26 cells. $*P < 0.05$ as compared with Colon26 (one way ANOVA). $n = 3$. B, Differential in vitro invasion activities. $*P < 0.05$ as compared with Colon26 (one way ANOVA). $n = 3$. C, Staining of invaded cells. Diff-Quick staining was carried out after invasion assay. Scale bars: 200 μm. D, The mRNA levels of MMP3 in the LuM1 cells transfected with siRNA. Relative mRNA levels normalized to *Gapdh* mRNA levels were shown. $*P < 0.05$ as compared with control si group. $\dagger P < 0.05$ as compared with MMP9 si group (one way ANOVA). $n = 3$. E, The mRNA levels of MMP9 in the LuM1 cells transfected with siRNA. Relative mRNA levels normalized to *Gapdh* mRNA levels were shown. $*P < 0.05$ as compared with control si group. $\dagger P < 0.05$ as compared with MMP3 si group (one way ANOVA). $n = 3$. F, Growth curves of LuM1 cells transfected with MMP-targeting or control siRNA. G and H, In vitro migration (G) and invasion (H) activities altered by MMP3 and/or MMP9 knockdown. Upper panels, quantified migration (G) and invasion (H) activities of LuM1 cells transfected with siRNA-targeting MMP3, MMP9, MMP3/MMP9, or the control dsRNA. $n = 5$. $*P < 0.05$ as compared to the control si group (one way ANOVA). Lower panels, migrated (G) and invaded (H) cells stained with Diff-Quick. Scale bars: 200 μm. Control si group, $n = 5$; MMP3 si group, $n = 5$; MMP9 si group, $n = 5$; MMP3/9 si group, $n = 6$. $*P < 0.05$ as compared to the control si group. $\dagger P < 0.05$ as compared to the MMP9 si group (one way ANOVA). Lower panel, Invaded cells stained with Diff-Quick. Scale bars: 200 μm

3.4 | The intracellular non-proteolytic PEX domain of MMP3 and the short MMP9 were expressed in the metastatic adenocarcinoma cells

We next examined expression and proteolytic activities of several isoforms of the MMPs produced from the metastatic LuM1 cells, and examined siRNA-mediated knockdown of these in vitro, based on that MMPs had been historically demonstrated as extracellular proteases, whereas non-proteolytic and intracellular roles for MMPs have been recently shown.[11,12] Therefore, prior to detection, we organized structures of MMP3 and MMP9 (Figures 4A and 4B). We examined isoforms of MMP3 produced in the LuM1 cells at by performing siRNA-mediated knockdown and subsequent Western blot analysis and zymography. (Full images of Western blot and zymography were shown in supplemental Figure S3). The

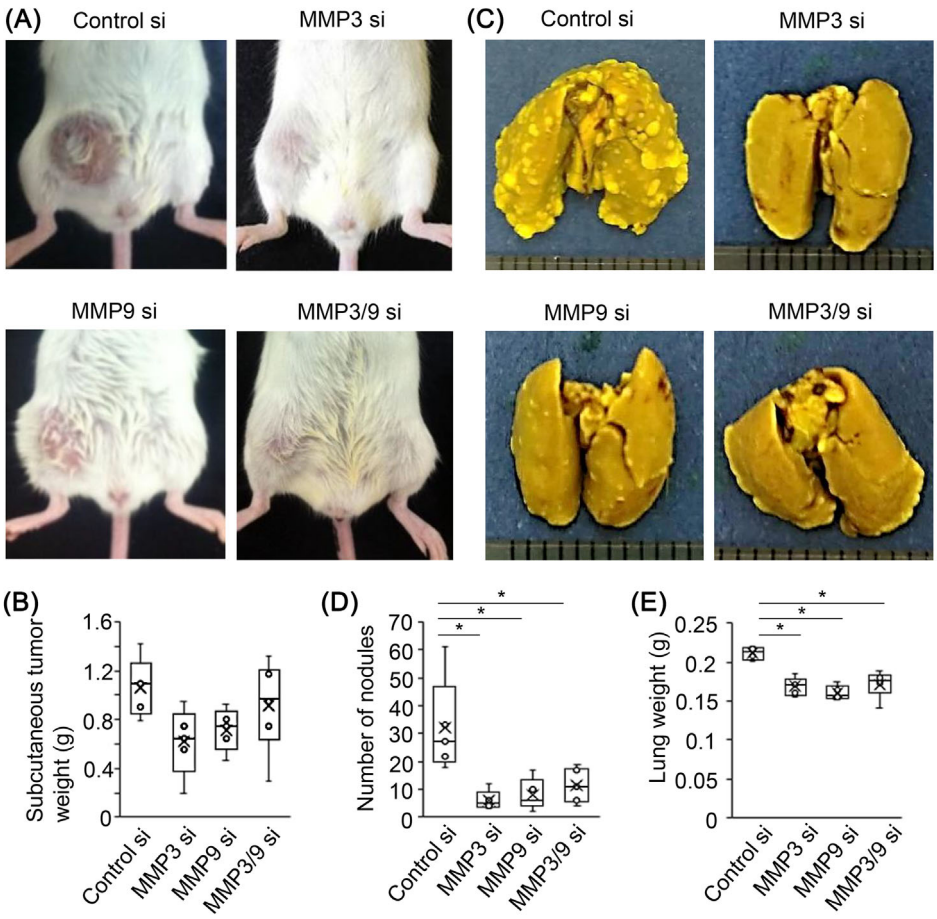

FIGURE 3 Targeting MMP3 and MMP9 attenuated tumor development and metastasis of the aggressive colon cancer cells. LuM1 cells transfected with siRNA targeting MMP3 and/or MMP9 or non-targeting dsRNA were subcutaneously injected to abdominal walls in mice. The primary tumors and the metastatic tumors in lungs were analyzed 20 days post-injection period. A, Representative images of mice bearing subcutaneous primary tumors. B, Weights of subcutaneous primary tumors. C, Representative images of lungs with metastatic tumor nodules. D, Numbers of metastatic tumor nodules in lungs. E, Weights of lungs with metastatic tumor nodules. C-E, Control si group, $n = 5$; MMP3 si group, $n = 5$; MMP9 si group, $n = 5$; MMP3/9 si group, $n = 6$. *$P < 0.05$, as compared to the control si group (one way ANOVA)

anti-PEX domain MMP3 antibody detected both full-length 54-kDa (arrow) and short 25-kDa PEX domain (arrowhead) of MMP3 (Figure 4C). The MMP9 siRNA increased the PEX of MMP3 and decreased full-length MMP3 (Figure 4C, compare lane 1 and lane 3), indicating crosstalk between MMP3 and MMP9. We next examined MMP3 proteolytic activity in the culture supernatant of the LuM1 cells in casein zymography. The 54-kDa and 100-kDa proteinases lysed casein, and these were thought to be proteolytic MMP3 monomer and dimer, respectively (Figure 4D, control si). The proteolytic MMP3 monomer was reduced by the MMP3 siRNA (arrow), whereas the proteolytic putative MMP3 dimer was not reduced by the MMP3 siRNA, but reduced by MMP3/MMP9 siRNA (arrowhead) (Figure 4D), indicating crosstalk between MMP3 and MMP9. As expected, the non-proteolytic 25-kDa PEX domain was not detected in the casein zymography.

We next examined isoforms of MMP9 produced from the LuM1 cells. Intracellular gelatinase activities of approx. 90-kDa and 250-kDa proteinases were significantly found in both lysate (Figure 4E) and culture supernatant (Figure 4F) of the metastatic LuM1 cells, but at much lower levels in the other low-metastatic cell lines. The 90-kDa gelatinase was thought to be MMP9 and the 250-kDa gelatinase was thought to be oligomers of MMP9.

We next examined knockdown of the intracellular and extracellular MMP9 produced by LuM1 cells. The anti-MMP9 antibody detected full-length (approx. 90-kDa, arrow), processed forms (64- and 67-kDa, arrowhead), and putative oligomer (250-kDa, asterisk) of MMP9 in the lysate of LuM1 cells (Figure 4G). Gelatinase activities of the 90-kDa MMP9 in the cell culture supernatant of LuM1 cells treated with the MMP9 siRNA was lower than that treated with the control siRNA or the MMP3 siRNA (Figure 4H).

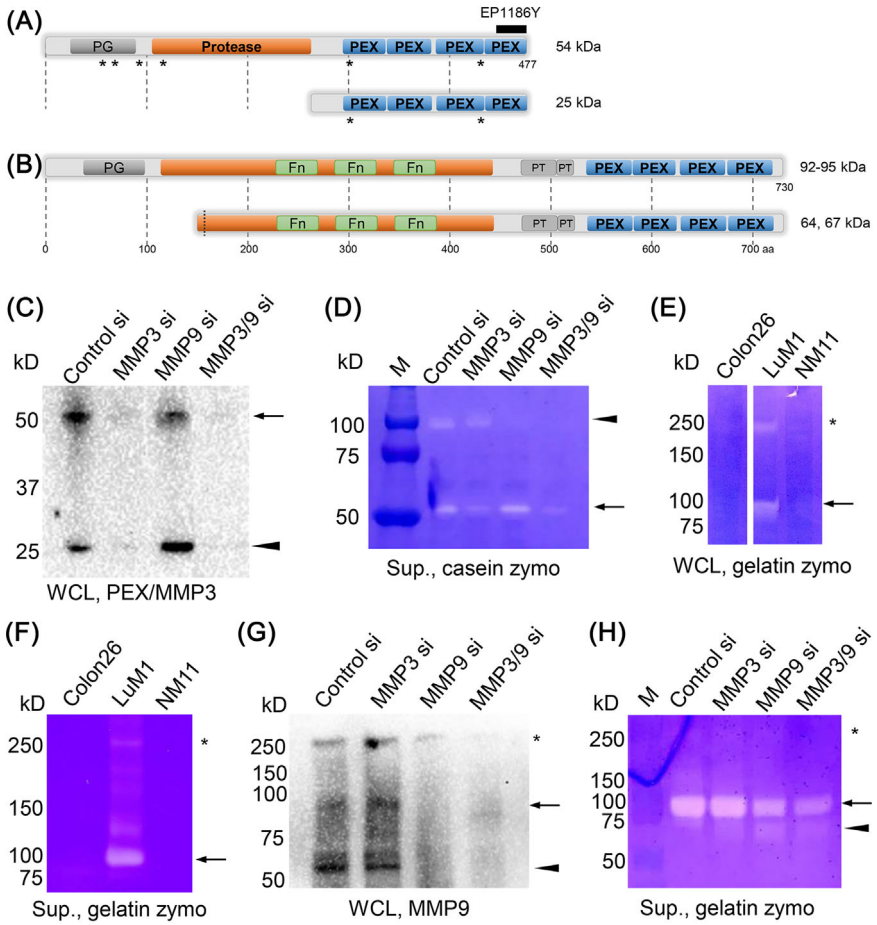

FIGURE 4 Knockdown of non-proteolytic and proteolytic, intracellular and extracellular MMP3 and MMP9. A, Schematic structures of murine MMP3. The structures of protease domain-containing 54-kDa MMP3 and non-proteolytic 25-kDa PEX domain of MMP3 are shown. The anti-PEX MMP3 antibody EP1186Y recognizes the epitope 450-477 position, which both the 54-kDa MMP3 and the 25-kDa PEX isoform contain. PG, peptide glycan binding domain. PEX, hemopexin-like repeat. Asterisks are positions of nuclear localization signals. B, Schematic structures of approx. 92-95-kDa MMP9 and 64- and 67-kDa MMP9. Fn, fibronectin type II domain. PT, PT repeat composed on the tetrapeptide xPTx. C, Western blot showing intracellular isoforms of MMP3 in the LuM1 cells and those knockdown. An arrow indicates full-length MMP3 (54-kDa). An arrowhead indicates the intracellular 25-kDa PEX isoform of MMP3. WCL, whole cell lysate. D, Casein zymography of extracellular isoforms of MMP3 and those knockdown in the LuM1 cells. An arrow indicates full-length MMP3 (54-kDa). An arrowhead indicates proteolytic MMP3 monomer or dimer. M, molecular weight marker. E, Intracellular gelatinase activities in the LuM1 cells. The WCLs prepared from LuM1, Colon26, and NM11 were examined in zymography. Gelatinase activities at approx. 90-kDa (arrow) and 250-kDa (asterisk) were seen. F, Extracellular gelatinase activities in the culture supernatant of the LuM1 cells. Gelatinase activities at approx. 90-kDa (arrow) and 250-kDa (asterisk) were seen. G, Western blot analysis of intracellular isoforms of MMP9 in the lysate of LuM1 cells and their knockdown. An arrow indicates approx. 90-kDa MMP9. An arrowhead indicates intracellular short MMP9 (64- and 67-kDa). An asterisk indicates putative intracellular oligomer of MMP9. H, Gelatin zymography of extracellular MMP9 and those knockdown in the LuM1 cells. Gelatinase activities were seen at approx. 90-kDa (arrow, the major band), 60-kDa (arrowhead), and 250-kDa (asterisk). M, molecular weight marker

These results indicate that the non-proteolytic PEX domain of MMP3 and the short MMP9 were intracellularly produced in the metastatic adenocarcinoma cells. The siRNAs targeting MMP3/9 successfully reduced proteolytic and non-proteolytic intracellular and extracellular isoforms of MMPs.

3.5 | Expression and nuclear localization of MMP3 in primary tumors and in metastatic lungs in allogeneic transplants

MMP3 was initially found as the first member of stromelysin, which lyse ECMs in stroma. Later studies have shown

intranuclear localization and roles of MMP3.[11,12] In the present study, *Mmp3* was notably expressed in the metastatic LuM1 in vitro. We next examined expression and subtumoral and subcellular localization of MMP3 in primary tumors and in lungs with metastatic tumors in an allogeneic transplant model. As it have been shown that the PEX domain of MMP3 has an essential role in transcriptional regulation,[12] we used an anti-PEX MMP3 antibody in immunohistochemistry. MMP3 was expressed at relatively high levels at marginal zone of tumor parenchyma (P) to stroma (S) in primary tumors, but at lower levels in central area of the parenchyma (Figures 5A and 5B). Notably, intranuclear MMP3 was found in both marginal parenchymal cells (arrowheads) and stromal cancer-associated fibroblast (CAF)-like cells (arrow) (Figure 5C).

We next examined subtumoral and subcellular localization of MMP3 in the metastatic lungs in the same model. MMP3-positive cells were found throughout the metastatic tumor nodules and in pulmonary alveolar locations (Figure 5E). MMP3 was found inside nuclei (arrow) and the nuclear margins (arrowhead) of cells with nuclear polyploidy in metastatic tumors in the lung (Figure 5F).

These results indicate that extra- and intracellular MMP3 involve CAF-related invasion, nuclear polyploidy, and metastasis of the aggressive adenocarcinoma cells.

3.6 | Nuclear PEX domain/MMP3 localized in tumor-stroma marginal area and MMP9 localized in central area of tumors

To more precisely investigate the nuclear localization of MMP3/9 in tumors, we next used immunofluorescence and confocal laser scanning microscopy and examined nuclear

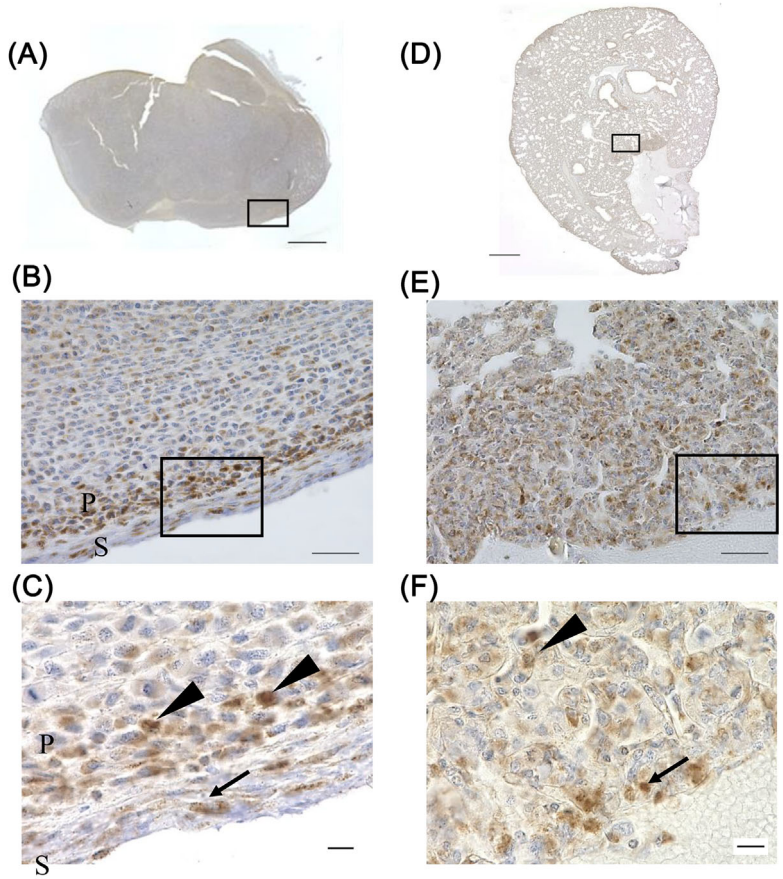

FIGURE 5 The subtumoral and subcellular localization of the PEX/MMP3 in primary tumors and in metastatic tumors in lungs. LuM1 cells were subcutaneously injected into abdominal walls in a mouse. A developed subcutaneous primary tumor (A-C) and a lung lesion (D-F) with metastatic tumor nodules were prepared at day 20 after the injection and then immunohistochemistry of the PEX/MMP3 was performed. A, A whole tumor. Scale bar: 500 μm. B, A magnified view of the box shown in A. Scale bar: 50 μm. C, A magnified view of the box shown in B. Scale bar: 10 μm. An arrow indicates MMP3 immunostained in a cancer-associated fibroblast (CAF)-like cell. Arrowheads indicate nuclear localization of MMP3. D, A whole lung with metastasis. Scale bar: 500 μm. E, A magnified view of the box shown in D. Scale bar: 50 μm. F, A magnified view of the box shown in E. Scale bar: 10 μm. An arrow indicates MMP3 accumulated in the nucleus. An arrowhead indicates MMP3 localization to the nuclear margin

MMP3/9 positive rate in each tumor area. We defined four areas of a tumor as follows: central (Figure 6A, left), interior, marginal, and stromal areas (Figure 6A, right). The rate of cells with nuclear MMP3 was most significant in the stromal area (17.6 %) and next in the tumor marginal area (9.4%) as compared to those in the interior (0.80 %) and central areas (0.73%) with the lower rate (Figure 6B-D). On the other hand, nuclear MMP9 positive cells were found notably in the central area (2.5 %) as compared to the other areas (Figures 6B and 6D).

We next assessed localization of MMP3 and MMP9 in a lung lesion with metastatic tumors. Tumor cells with nuclear MMP3/9 appeared to scatter throughout the metastatic cancer nodule in the lung and in pulmonary alveolar locations (Figure 6E), consisting with IHC data shown in Figure 5.

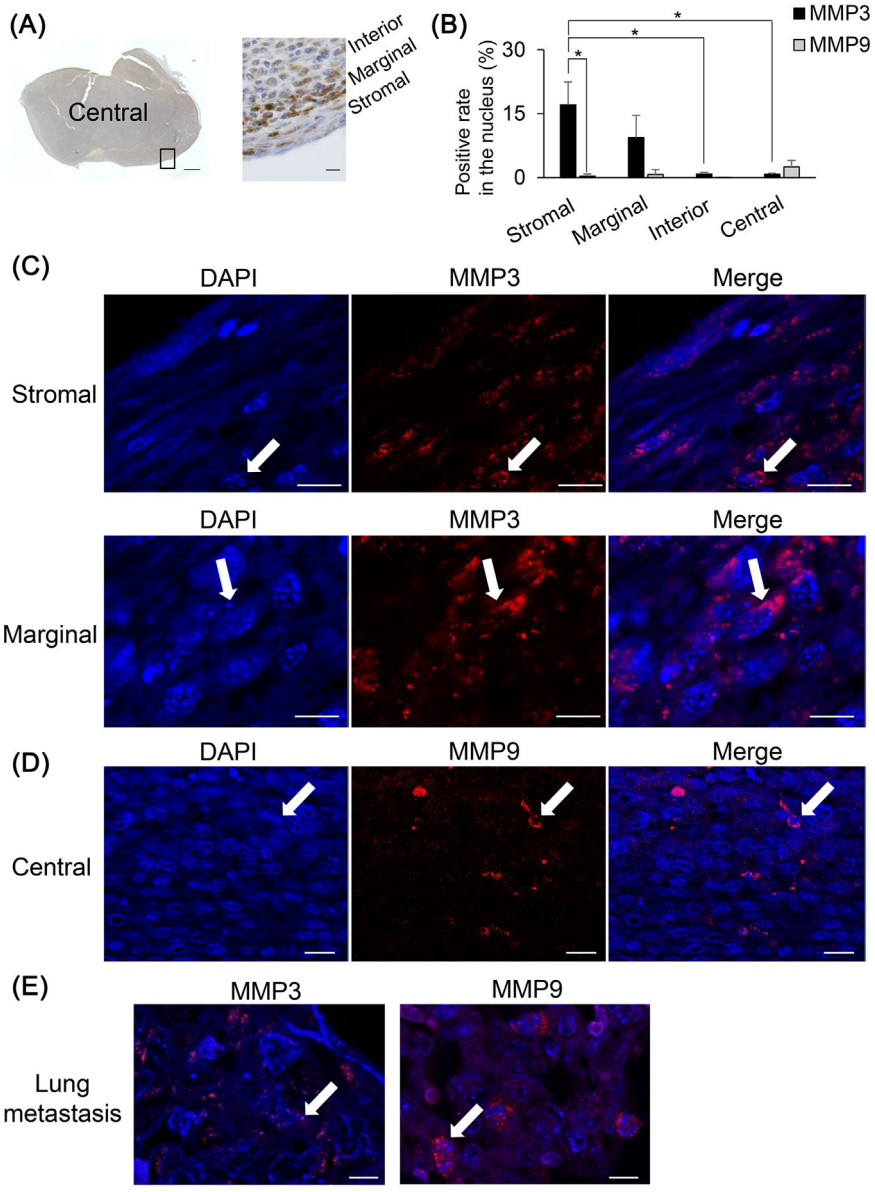

FIGURE 6 The nuclear PEX/MMP3 found in tumor-stroma marginal area and nuclear MMP9 in tumor central area. For immunostaining, an anti-PEX MMP3 antibody and anti-MMP9 full-length were used. A, The scheme of definition of the central area (shown in the left photomicrograph), interior, marginal, and stromal areas (shown in the right photomicrograph) of a tumor. Scale bars, 500 μm (left) and 10 μm (right). The area in the rectangle in the left image was shown with a high power magnification in the right image. B, The positive rate of MMP3 and MMP9 in the nuclei in individual area. n = random three fields. $^*P < 0.05$ as compared to the nuclear MMP3 positive rate in the stromal area. C and D, Confocal microscopy of subtumoral and subcellular localization of MMP3 (C) and MMP9 (D). Red, MMP3 or MMP9. Blue, DNA stained with DAPI. Arrows indicate the MMP3 or MMP9 localization in the nuclei. Scale bars, 10 μm (C) and 20 μm (D). E, Confocal microscopy of subcellular localization of MMP3/9 in the lung lesion with metastatic cancer cells. Arrows indicate MMP3 (left) and MMP9 (right) positive region in the nuclei. Scale bars, 5 μm

Of note, DNA stained with DAPI appeared to be dot-like condensation in cell nuclei in both primary and metastatic tumors (Figure 6C-E), indicating chromosomal condensation involving gene regulation. MMP3 and MMP9 appeared to co-localize with DNA (Figure 6C-E, arrows), suggesting DNA-binding and gene regulation. MMP3 and MMP9 appeared to localize out of nuclei-cytoplasm or extracellular region as well.

These results indicate that nuclear PEX domain/MMP3 localized in primary tumor-stroma marginal area and lung-metastatic tumor nodules. Nuclear MMP9 localized in central area of primary tumors and in lung-metastatic tumor nodules.

3.7 | Overexpression of the PEX-domain promotes proliferation and migration of the metastatic cancer cells

We next asked whether the non-proteolytic PEX domain could alter proliferation, migration, and invasion of the aggressively metastatic cancer cells. Overexpression of the PEX of MMP3 significantly increased proliferation of LuM1 cells (Figure 7A). Of note, overexpression of the PEX increased migration of LuM1 cells to 204% level of the control (Figure 7B). Overexpression of the PEX tended to increase invasion of LuM1 cells to 127.1% level of the control (Figure 7C), suggesting that protease activities of MMPs might promote invasion rather than the non-proteolytic PEX.

These results indicate that the PEX-domain has key roles in abilities of proliferation and migration of the metastatic adenocarcinoma cells.

4 | DISCUSSION

MMP family members are consist of secretory types (collagenases, gelatinases, stromelysins) and membrane types (MT-MMPs) and have crucial roles in the progression of diseases, including cancer, arthritis, and periodontitis. Most metalloproteinase inhibitors had been designed and, indeed, to block catalytic pockets that possess a zinc ion and proteinase activity. However, any metalloproteinase inhibitor has been approved for clinical application. Recent studies, including the present study, have shown intracellular and non-proteolytic roles for MMPs in arthritis and cancer.[11–13] In addition to in an arthritis model and in a chondrosarcoma-

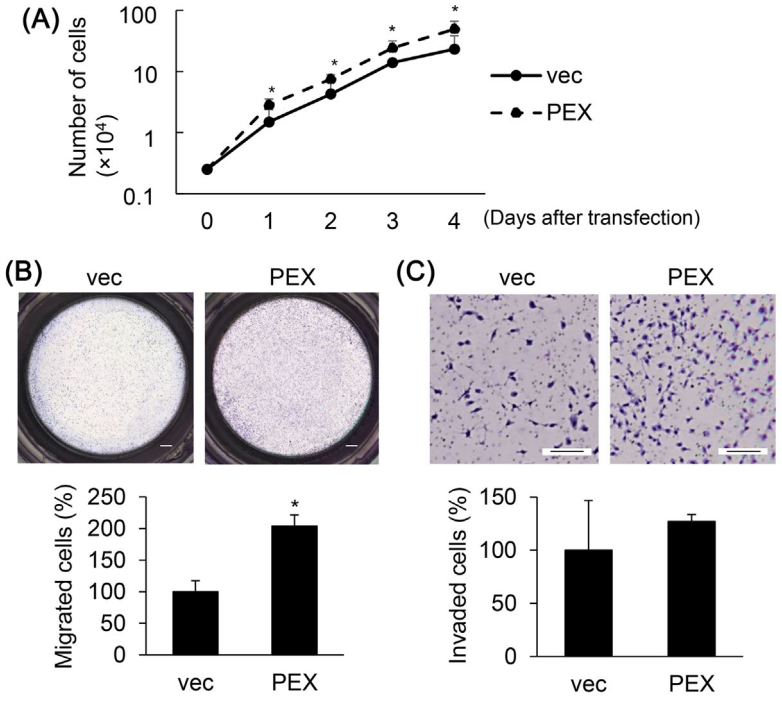

FIGURE 7 The potent roles of the PEX-domain in proliferation and migration of the metastatic cancer cells. A, Growth curves of the metastatic LuM1 cells transfected with pFlag3-PEX-myc or the control vector. $*P < 0.05$ as compared with control vector. B, In vitro migration activities altered by overexpression of the PEX domain. Upper panels, staining of the migrated cells. Scale bars: 200 μm. Lower panel, ratio of migrated cells upon overexpression of the PEX domain or the control vector. $n = 3$. $*P < 0.05$ as compared with control vector. C, In vitro invasion activities. Upper panels, staining of the invaded cells. Scale bars: 100 μm, Lower panel, ratio of the invaded cells upon overexpression of the PEX domain or the control vector. $n = 3$

derived cell line,[11] nuclear MMP3 was significantly found in primary tumors and in metastatic sites in allogeneic transplant model of the aggressive adenocarcinoma cells (Figures 5 and 6). Both the PEX isoform and full-length MMP3 were significantly found in the metastatic LuM1 cells (Figure 4). The siRNA targeting MMP3 reduced both 25-kDa PEX isoform and 54-kD full-length MMP3 (Figure 4C) and simultaneously attenuated proliferation and migration of the aggressive adenocarcinoma cells (Figures 2F and 2G). On the other hand, overexpression of the PEX isoform promoted proliferation and migration of the LuM1 cells (Figure 7). Therefore, the PEX isoform and domain are responsible for MMP-driven cell proliferation, migration, and subsequent metastasis of the aggressive adenocarcinoma cells.

MMP3 and MMP9 colocalized with DNA in subcutaneous tumors in vivo (Figure 6). These data indicated potential roles for MMP3 and MMP9 in gene regulation in primary and metastatic tumors. We showed that MMP3 localized in cell nuclei in stroma-tumor marginal cells in subcutaneous tumors (Figures 5B, 5C and 6B, 6C), suggesting that MMP3 involves potential tumor-stromal interaction such as induction of CAFs, migration, invasion, and tumor angiogenesis, tumor-immunology interaction through the stroma. In contrast, MMP9 was localized in central area of subcutaneous tumors (Figures 6B and 6D). Central area of tumors are often necrotic and/or hypoxic where hypoxia-inducible transcription factor (HIF1) controls transcription of target genes, including MMP genes[23] and stem cell genes.[22,24–26] We previously showed that MMPs and CTGF/CCN2 were inducible upon hypoxia through distinctive mechanisms.[23] MMP9 is one of key proteins induced by HIF1 in tumors whereas CTGF could be increased through mRNA stabilization.[23] Thus, HIF1, MMP9, and CTGF can be co-increased at central area of tumors and the induced MMP9 and CTGF can promote tumor angiogenesis.[23] CTGF may be increased by transcriptional role for MMP9 in central area of tumors (Figure 6D), in addition to the role for MMP3 in transcription.[11,12] Indeed, mRNA levels of CTGF were altered in tumors in vivo upon knockdown of MMP3 and MMP9 (data not shown). Thus, we are further investigating mechanisms underlying MMPs regulation of CTGF and HSPs that may mediate tumor progression and metastasis.

In addition to the intracellular and non-catalytic roles for MMP3 as shown above, intracellular and non-catalytic MMP9 was suggested in the present study. The approx. 60-kDa MMP9 isoforms were significantly detected in the lysate of the metastatic LuM1 cells (Figure 4G). However, any intracellular proteolytic activity of the 60-kDa MMP9 was not detected in the lysate of LuM1 cells, even though the gelatinase activities of 90-kDa and 250-kDa MMP9 were found (Figure 4F) and extracellular proteinase activity of 60-kDa MMP9 was detected in the cell culture supernatant (Figure 4H). Thus, the intracellular 60-kDa MMP9 does not possess any proteolytic activity or some intracellular factors such as DNA/chromatin might mask the proteinase domain.

Of note, the non-proteolytic MMPs cannot be directly targeted by metalloproteinase inhibitors that block proteolytic pockets. Moreover, the intranuclear MMPs might be difficult to be accessed by small molecule drugs, which can be excreted from cancer cells, and are much more difficult by molecularly targeted antibody drugs, which are too large to enter into cells and nuclei. The siRNA-mediated knockdown tested in the present study significantly and sustainably reduced intracellular and extracellular, non-catalytic and catalytic MMPs (Figure 4, S3). These efficient knockdown of various isoforms of MMPs might involve their efficient effects to attenuate migration, invasion, and metastasis. The RNAi approaches are able to target mRNAs that fundamentally encode proteins that are post-translationally modified, processed, and localized to specific regions. Thus, the RNAi approaches might be more fundamentally effective in disease therapies.

It was recently reported that MMP3 functions in a coordinated manner with a chemokine, IL-8/CXCL8, expressed in melanoma via direct regulation by NFAT1, thus promoting tumor progression and metastasis.[27] Another recent study found that interleukin-regulatory transcription factor 8 (IRF-8) directly repressed the *Mmp3* gene in relatively mild mammary tumor cells, whereas loss of IRF-8 in coordination with gain in *Mmp3* expression promoted tumor progression and metastasis.[28] These studies were done using xenotransplantation of human cancer cells into immunodeficient mice. We consider that the present protocol of allogeneic transplantation into an immunologically genetically relatively normal host will be useful for further studies of tumor microenvironment and immunology.

Thus, intracellular and non-proteolytic MMPs have crucial roles in cancer progression. The versatile RNAi approach is able to reduce intracellular and extracellular, non-proteolytic and proteolytic MMPs at once and thus appears to be significantly effective to attenuate various aspects of cancer progression, including proliferation, migration, and invasion of cancer cells, tumor development and metastasis.

ACKNOWLEDGMENTS

This paper is dedicated to the memory of one of the coauthors, Professor Ken-ichi Kozaki, who passed away on May 29, 2016. The authors thank Kisho Ono, Toshifumi Fujiwara, Yuri Namba, Tomoko Yamamoto and Kazumi Ohyama for their technical assistance and useful discussion. This work was supported by JSPS KAKENHI, grant numbers JP17K17895 (to YO), JP17K11642 (to TE), JP26293067 (to KK), JP26670815 (to KK), Start-up Grant for Young Scientists at Okayama Univ. (to YO), Molecular Imaging Micro Dose Phase 0 Grant at Okayama Univ. (to YO and

KK), Gender Equality Grant at Okayama Univ. (to YO), and a Ryobi Teien Memorial Foundation Grant (to TE).

CONFLICTS OF INTEREST

The authors have no competing financial interests to declare.

REFERENCES

1. Nowell PC. The clonal evolution of tumor cell populations. *Science*. 1976;194:23–28.
2. Greaves M, Maley CC. Clonal evolution in cancer. *Nature*. 2012;481:306–313.
3. Kreso A, Dick JE. Evolution of the cancer stem cell model. *Cell Stem Cell*. 2014;14:275–291.
4. Kessenbrock K, Plaks V, Werb Z. Matrix metalloproteinases: regulators of the tumor microenvironment. *Cell*. 2010;141:52–67.
5. Kessenbrock K, Dijkgraaf GJ, Lawson DA, et al. A role for matrix metalloproteinases in regulating mammary stem cell function via the Wnt signaling pathway. *Cell Stem Cell*. 2013;13:300–313.
6. Radisky DC, Levy DD, Littlepage LE, et al. Rac1b and reactive oxygen species mediate MMP-3-induced EMT and genomic instability. *Nature*. 2005;436:123–127.
7. Sato H, Takino T, Okada Y, et al. A matrix metalloproteinase expressed on the surface of invasive tumour cells. *Nature*. 1994;370:61–65.
8. Vandenbroucke RE, Libert C. Is there new hope for therapeutic matrix metalloproteinase inhibition? *Nat Rev Drug Discov*. 2014;13:904–927.
9. Hashimoto G, Inoki I, Fujii Y, Aoki T, Ikeda E, Okada Y. Matrix metalloproteinases cleave connective tissue growth factor and reactivate angiogenic activity of vascular endothelial growth factor 165. *J Biol Chem*. 2002;277:36288–36295.
10. Prenzel N, Zwick E, Daub H, et al. EGF receptor transactivation by G-protein-coupled receptors requires metalloproteinase cleavage of proHB-EGF. *Nature*. 1999;402:884–888.
11. Eguchi T, Kubota S, Kawata K, et al. Novel transcription-factor-like function of human matrix metalloproteinase 3 regulating the CTGF/CCN2 gene. *Mol Cell Biol*. 2008;28:2391–2413.
12. Eguchi T, Calderwood SK, Takigawa M, Kubota S, Kozaki KI. Intracellular MMP3 promotes HSP gene expression in collaboration with chromobox proteins. *J Cell Biochem*. 2017;118:43–51.
13. Eguchi T, Kubota S, Kawata K, et al. 2010. *Novel transcriptional regulation of CCN2/CTGF by nuclear translocation of MMP3*. Dordrecht, Nertherlands: Springer, pp 255–264.
14. Yang Y, Candelario-Jalil E, Thompson JF, et al. Increased intranuclear matrix metalloproteinase activity in neurons interferes with oxidative DNA repair in focal cerebral ischemia. *J Neurochem*. 2010;112:134–149.
15. Mehner C, Miller E, Khauv D, et al. Tumor cell-derived MMP3 orchestrates Rac1b and tissue alterations that promote pancreatic adenocarcinoma. *Mol Cancer Res*. 2014;12:1430–1439.
16. Hyuga S, Nishikawa Y, Sakata K, et al. Autocrine factor enhancing the secretion of M(r) 95,000 gelatinase (matrix metalloproteinase 9) in serum-free medium conditioned with murine metastatic colon carcinoma cells. *Cancer Res*. 1994;54:3611–3616.
17. Sakata K, Kozaki K, Iida K, et al. Establishment and characterization of high- and low-lung-metastatic cell lines derived from murine colon adenocarcinoma 26 tumor line. *Jpn J Cancer Res (Cancer Sci)*. 1996;87:78–85.
18. Tsuruo T, Yamori T, Naganuma K, Tsukagoshi S, Sakurai Y. Characterization of metastatic clones derived from a metastatic variant of mouse colon adenocarcinoma 26. *Cancer Res*. 1983;43:5437–5442.
19. Ma O, Cai WW, Zender L, et al. MMP13, Birc2 (cIAP1), and Birc3 (cIAP2), amplified on chromosome 9, collaborate with p53 deficiency in mouse osteosarcoma progression. *Cancer Res*. 2009;69:2559–2567.
20. Sousa NG, Cardoso CR, Silva JS, Kuga MC, Tanomaru-Filho M, Faria G. Association of matrix metalloproteinase inducer (EMMPRIN) with the expression of matrix metalloproteinases-1, -2 and -9 during periapical lesion development. *Arch Oral Biol*. 2014;59:944–953.
21. You S, Avidan O, Tariq A, et al. Role of epithelial-mesenchymal transition in repair of the lacrimal gland after experimentally induced injury. *Invest Ophthalmol Vis Sci*. 2012;53:126–135.
22. Eguchi T, Sogawa C, Okusha Y, et al. Organoids with cancer stem cell-like properties secrete exosomes and HSP90 in a 3D Nano-Environment. *PLoS ONE*. 2018;13:0191109.
23. Kondo S, Kubota S, Shimo T, et al. Connective tissue growth factor increased by hypoxia may initiate angiogenesis in collaboration with matrix metalloproteinases. *Carcinogenesis*. 2002;23:769–776.
24. Keith B, Simon MC. Hypoxia-inducible factors, stem cells, and cancer. *Cell*. 2007;129:465–472.
25. Keith B, Johnson RS, Simon MC. HIF1alpha and HIF2alpha: sibling rivalry in hypoxic tumour growth and progression. *Nat Rev Cancer*. 2011;12:9–22.
26. Semenza GL. The hypoxic tumor microenvironment: a driving force for breast cancer progression. *Biochim Biophys Acta*. 2016;1863:382–391.
27. Shoshan E, Braeuer RR, Kamiya T, et al. NFAT1 directly regulates IL8 and MMP3 to promote melanoma tumor growth and metastasis. *Cancer Res*. 2016;76:3145–3155.
28. Banik D, Netherby CS, Bogner PN, Abrams SI. MMP3-mediated tumor progression is controlled transcriptionally by a novel IRF8-MMP3 interaction. *Oncotarget*. 2015;6:15164–15179.

SUPPORTING INFORMATION

Additional supporting information may be found online in the Supporting Information section at the end of the article.

How to cite this article: Okusha Y, Eguchi T, Sogawa C, et al. The intranuclear PEX domain of MMP involves proliferation, migration, and metastasis of aggressive adenocarcinoma cells. *J Cell Biochem*. 2018;1–14. https://doi.org/10.1002/jcb.27040